


# Microscopic 3-dimensional mapping of hydrogen bubbles in polycrystalline Al by elastic recoil detection analysis under transmission geometry

Cite as: AIP Advances 9, 105111 (2019); <https://doi.org/10.1063/1.5099528>

Submitted: 11 April 2019 . Accepted: 04 October 2019 . Published Online: 11 October 2019

A. Yamazaki, K. Sasa , S. Tomita, S. Ishii, H. Naramoto, M. Sataka, H. Kudo, G. Itoh, and M. Ohkubo 

## COLLECTIONS

Paper published as part of the special topic on [Chemical Physics](#), [Energy, Fluids and Plasmas](#), [Materials Science](#) and [Mathematical Physics](#)



View Online



Export Citation



CrossMark

## ARTICLES YOU MAY BE INTERESTED IN

[Effect of admixing graphene oxide on abrasion resistance of ordinary portland cement concrete](#)

AIP Advances 9, 105110 (2019); <https://doi.org/10.1063/1.5124388>

[Numerical study of amplitude modulation in the atmospheric boundary layer at very high Reynolds number](#)

AIP Advances 9, 105112 (2019); <https://doi.org/10.1063/1.5125566>

[Novel concept for VCSEL enhanced silicon photonic coherent transceiver](#)

AIP Advances 9, 105114 (2019); <https://doi.org/10.1063/1.5120019>



## NEW: TOPIC ALERTS

Explore the latest discoveries in your field of research

[SIGN UP TODAY!](#)

# Microscopic 3-dimensional mapping of hydrogen bubbles in polycrystalline Al by elastic recoil detection analysis under transmission geometry

Cite as: AIP Advances 9, 105111 (2019); doi: 10.1063/1.5099528

Submitted: 11 April 2019 • Accepted: 4 October 2019 •

Published Online: 11 October 2019





View Online



Export Citation



CrossMark

A. Yamazaki,<sup>1</sup> K. Sasa,<sup>1,2,a)</sup>  S. Tomita,<sup>1</sup> S. Ishii,<sup>2</sup> H. Naramoto,<sup>2</sup> M. Sataka,<sup>2</sup> H. Kudo,<sup>2</sup> G. Itoh,<sup>3</sup> and M. Ohkubo<sup>1,4</sup> 

## AFFILIATIONS

<sup>1</sup>Faculty of Pure and Applied Sciences, University of Tsukuba, 1-1-1 Tennodai, Tsukuba, Ibaraki 305-8571, Japan

<sup>2</sup>Research Facility Center for Science and Technology, University of Tsukuba, 1-1-1 Tennodai, Tsukuba, Ibaraki 305-8577, Japan

<sup>3</sup>Department of Mechanical Engineering, College of Engineering, Ibaraki University, 4-12-1, Nakanarusawa, Hitachi, Ibaraki 316-8511, Japan

<sup>4</sup>National Institute of Advanced Industrial Science and Technology (AIST), 1-1-1 Umezono, Tsukuba, Ibaraki 305-8568, Japan

<sup>a)</sup>Corresponding author E-mail address: [ksasa@tac.tsukuba.ac.jp](mailto:ksasa@tac.tsukuba.ac.jp)

## ABSTRACT

We have measured microscopic 3-dimensional distribution of plasma-charged hydrogen in polycrystalline Al. The measurements have been carried out nondestructively by using elastic recoil detection analysis under transmission geometry of a collimated 8 MeV  $^4\text{He}^{2+}$  beam. The recoil cross section as large as  $2 \times 10^3$  mb/sr due to the nuclear elastic collision allowed observation of the spatial distribution of hydrogen in the Al sample of 80  $\mu\text{m}$  thickness. The distribution maps of hydrogen clearly visualize hydrogen bubbles of 10–20  $\mu\text{m}$  diameter in the surface layer of about 12  $\mu\text{m}$  thickness. The critical concentration of hydrogen minimally needed for growth of the hydrogen bubble of ten- $\mu\text{m}$  size has been determined to be  $1.6 \times 10^{20}$   $\text{cm}^{-3}$ .

© 2019 Author(s). All article content, except where otherwise noted, is licensed under a Creative Commons Attribution (CC BY) license (<http://creativecommons.org/licenses/by/4.0/>). <https://doi.org/10.1063/1.5099528>

## I. INTRODUCTION

Hydrogen can seriously affect physical, and especially, mechanical properties of materials, as reviewed in the literatures.<sup>1,2</sup> Knowledge of hydrogen behavior in materials, for example, related to hydrogen embrittlement, is extremely required for structural materials used under severe environments. In many cases, the hydrogen-induced phenomena accompany migration and accumulation of hydrogen in materials. However, such behavior of hydrogen is not fully understood yet mainly because of the difficulty in sensitive detection of hydrogen.<sup>3,4</sup> For other atom species, elemental analyses based on atomic transitions are widely used, but these are not effective for direct detection of hydrogen in a surrounding medium of much heavier elements. Not only direct detection of hydrogen, but also microscopic visualization of 3-dimensional hydrogen distribution in solids is

necessary for research and development of hydrogen-containing materials.

For this purpose, it is suitable to employ the collision process between the incident fast ion and hydrogen nucleus. This is advantageous for micrometer-scale analysis compared, for example, with neutron tomography having lower spatial resolution by a factor of ten.<sup>5</sup> In fact, hydrogen mapping has been carried out by using H–H scattering to observe localized hydrogen at a grain boundary in diamond,<sup>6</sup> and to analyze trapping of implanted hydrogen in tungsten.<sup>7</sup> In many cases, however, the quality of hydrogen mapping using ion beams is seriously restricted by weak hydrogen signals. Improved signal statistics are needed for practical analysis, especially for mapping of hydrogen in materials.

In the present work, elastic recoil detection analysis under transmission geometry (T-ERDA) has been applied to observe hydrogen distribution in polycrystalline Al. Microscopic behavior of

hydrogen in Al attracts much attention because of the lack of knowledge about influence of incorporated hydrogen on the mechanical properties of Al and Al-alloys. Several kinds of approaches have been carried out to investigate the microscopic behavior of hydrogen in Al, for example, using X-ray diffraction and small-angle scattering of X-rays and neutrons,<sup>8,9</sup> thermal desorption spectroscopy,<sup>10</sup> X-ray computed tomography,<sup>11</sup> and secondary ion mass spectroscopy.<sup>3</sup> In these analyses, the object to be detected is not hydrogen itself situating in the Al matrix. Therefore, T-ERDA is expected to provide direct information on the behavior of hydrogen in Al.

## II. EXPERIMENTS

In T-ERDA, a particle detector is set on the ion-beam axis and a thin sample is placed in front of the detector. The present T-ERDA relies on the larger stopping power for He than for H.<sup>12</sup> The thickness of the Al sample is chosen so that incident He is stopped in the sample, i.e., greater than the (projected) range of He in Al, whereas recoiling H passes through the sample and goes into the particle detector. Since incident He and recoiling H undergo energy loss in the sample, the kinetic energy of detected H depends on the depth where the hydrogen atom originally was. Actually, the recoil at shallower surface layer results in the detection of H with higher kinetic energy. The maximum detectable depth for hydrogen is determined from the condition that the recoiling H has zero kinetic energy after passing through the sample. Figure 1 schematically shows T-ERDA in the present case, which is based on the numerical table of stopping and range of ions in matter.<sup>13</sup>

We prepared pure (99.99%) annealed Al foils of typically  $1 \times 2 \text{ cm}^2$  size and  $110 \text{ }\mu\text{m}$  thickness. They were charged with hydrogen under relatively severe plasma conditions (for example, at  $780 \text{ V}$  for 3 hours) and electro-polished to remove the hydrogen blisters formed on the surface. The final thickness of the foils thus obtained for T-ERDA samples was much less than  $110 \text{ }\mu\text{m}$ . These samples are expected to contain  $\text{H}_2$  bubbles, according to the literatures.<sup>9–11</sup> Figure 2 shows an optical photograph of the Al sample taken with vertical illumination. Accordingly, the white images here and there are due to the reflected light in the  $180^\circ$  direction, indicating the rough Al surface. This is in contrast to the apparently flat surface of the Al-coated mylar which is set for reference of a hydrogen-containing sample. Because of such roughness, we have carefully selected the surface area where the measured distribution

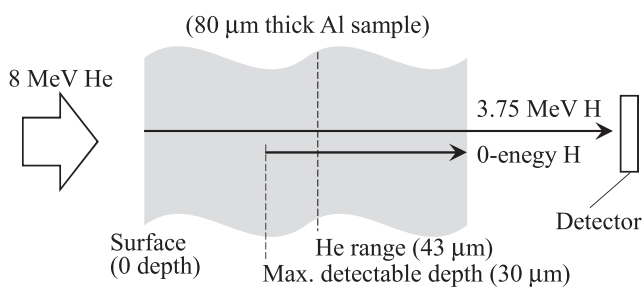


**FIG. 1.** Schematic diagram of the present T-ERDA. Deeper H recoil results in lower exit energy.

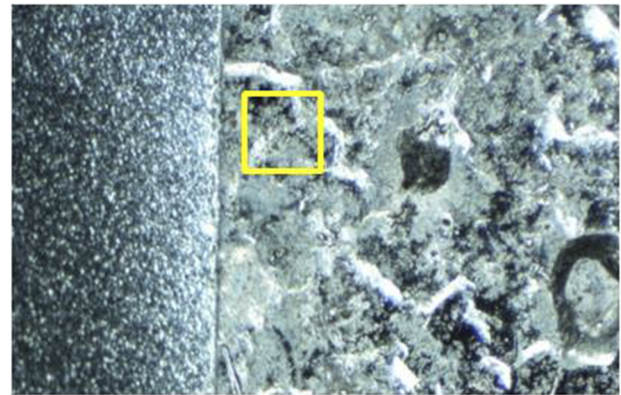


**FIG. 2.** Optical photograph of the surface of the Al sample placed on the right. The Al-coated mylar film placed on the left is for reference of a hydrogen-containing sample. The square marked in yellow shows the  $250 \times 250 \text{ }\mu\text{m}^2$  area analyzed by T-ERDA.

of hydrogen seems typical and also demonstrative of the present 3-dimensional mapping.

An 8-MeV  $^4\text{He}^{2+}$  beam was collimated to  $3.5 \text{ }\mu\text{m}$  diameter and was incident on the Al sample by using the microbeam system installed at the 6MV electrostatic tandem accelerator at the University of Tsukuba.<sup>12</sup> The distance from the Al sample to the particle detector of 8 mm diameter was 14.6 mm, which provides the acceptable recoil angle of  $0$  to  $15.3^\circ$ . Under the pressure of  $\sim 10^{-5} \text{ Pa}$ , we measured energy spectra for  $128 \times 128$  beam spots while scanning the collimated He beam step-by-step to cover the selected  $250 \times 250 \text{ }\mu\text{m}^2$  area on the sample. The measurement time for accumulating the  $128 \times 128$  spectra was about 1 hour. Even after repeating the above measurement for 5 times at the same beam spot on the sample, there was no noticeable change in the spectra, implying negligible influence of the He irradiation during the experiments. Furthermore, the measurements were carried out for several areas on the sample to confirm the consistency of analysis results.

For a hard collision of  $^4\text{He}$  against  $^1\text{H}$ , the recoil cross section has a maximum at the incident He energy of 8–10 MeV.<sup>12,14,15</sup> Indeed, the differential recoil cross section at recoil angles of  $0$ – $15.3^\circ$  amounts to approximately  $2 \times 10^3 \text{ mb/sr}$  in the laboratory frame which is greater by a factor of 300–400 than for the Coulomb field only. Such a maximum is characteristic of the nuclear elastic scattering which is typical for the relatively high-energy collisions like in the present case. The use of nuclear elastic scattering is therefore advantageous to improve the signal statistics of hydrogen mapping.

## III. RESULTS AND DISCUSSION

Several considerations are necessary for better understanding of the measured 3-dimensional image of hydrogen. To do this, discussion starts with Fig. 3, showing the energy spectrum which is obtained by summing over the  $128 \times 128$  spectra for the H-charged Al sample of  $80 \text{ }\mu\text{m}$  thickness. The investigated area on the sample is shown in Fig. 2 with the square marked in yellow. The 3.75 MeV energy at the origin of depth scale inserted in Fig. 3

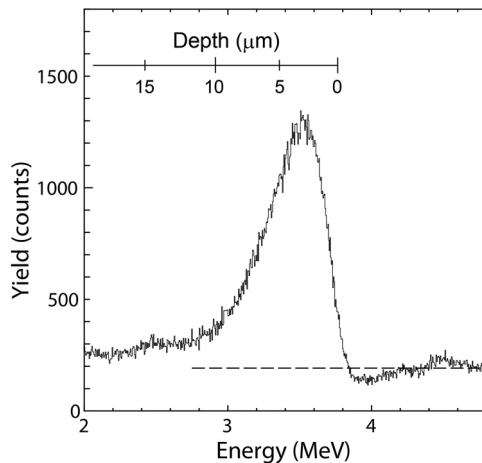


**FIG. 3.** T-ERDA energy spectrum measured for the  $250 \times 250 \mu\text{m}^2$  area on the Al sample. The scale of depth where the H recoil occurred is indicated. The dashed line shows the assumed background of 192 counts.

corresponds to the recoil occurring on the Al surface. This was determined from the high-energy edge of the spectrum for a spot area chosen from the  $250 \times 250 \mu\text{m}^2$  area, where hydrogen is localized near the surface. The high-energy edge also allowed to estimate the depth resolution of  $\sim 1.2 \mu\text{m}$  in the present analysis. The non-zero yield at energies higher than 4 MeV indicates existence of background under the hydrogen yield. This background is believed to stem from the nuclear reactions of  $^4\text{He}$  and Al since no such background was observed for a Ni foil with higher Coulomb barrier. The dashed line shows the assumed background of 192 counts (per channel) which is the average yield in the 4.0–4.8 MeV energy range.

In Fig. 3, the hydrogen yield is given by subtracting the background yield from the spectrum yield. It follows that the hydrogen yield is recognized predominantly from the surface to the depth of  $12 \mu\text{m}$ . It is important to note that the maximum detectable depth of  $30 \mu\text{m}$  in the present case is greater than  $12 \mu\text{m}$ , which certainly assures absence of hydrogen beyond the  $12 \mu\text{m}$  depth. The total hydrogen yield  $Y = 118937$  counts, obtained by integrating the hydrogen yield in the 0– $12 \mu\text{m}$  range, is expressed as

$$Y = N\rho \int \frac{d\sigma}{d\Omega} d\Omega = N\rho \int_0^{\varphi_0} \frac{d\sigma}{d\Omega} 2\pi \sin\varphi d\varphi, \quad (1)$$

where  $N$  is the number of incident He,  $\rho$  is the areal density of hydrogen when the Al sample is viewed along the beam direction,  $d\sigma/d\Omega$  is the differential recoil cross section in the laboratory frame as a function of solid angle  $\Omega$ , and  $\varphi$  is the recoil angle. Notably, Eq. (1) is on the basis of the fact that the counting efficiency of the particle detector is effectively 100%. In the present case,  $N = 9.0 \times 10^{11}$  (for 80 pA  $\text{He}^{2+}$  and the measurement time of 3600 s), and  $\varphi_0 = 15.3^\circ$ . Also, the integral in Eq. (1) can be evaluated with the numerical table of recoil cross sections given by IBANDL,<sup>14</sup> thereby we obtain  $3.35 \times 10^{-25} \text{cm}^2$  for 7.6 MeV He which is responsible for the main H yield at 3.5 MeV in Fig. 3. These values lead to  $\rho = 3.94 \times 10^{17} \text{cm}^{-2}$  for the Al sample. By assuming the thickness of the hydrogen-charged layer  $t = 12 \mu\text{m}$ , the average hydrogen concentration  $n_{\text{av}} = \rho/t = 3.3 \times 10^{20} \text{cm}^{-3}$  has been determined, which corresponds to 0.55% of the atomic density of polycrystalline Al.

Figure 4 consisting of 6 maps shows 3-dimensional hydrogen mapping of the  $250 \times 250 \mu\text{m}^2$  area, marked with the yellow square in Fig. 2. In these 6 maps, the measured yield for each 2- $\mu\text{m}$  slice of the depth, labeled with (a)–(f), was taken from the  $128 \times 128$  energy spectra. The yield is shown in the logarithmic color scale for later discussion of the low uniform yield. In this mapping, the lateral resolution is equal to the beam size of  $3.5 \mu\text{m}$ , and the depth resolution is

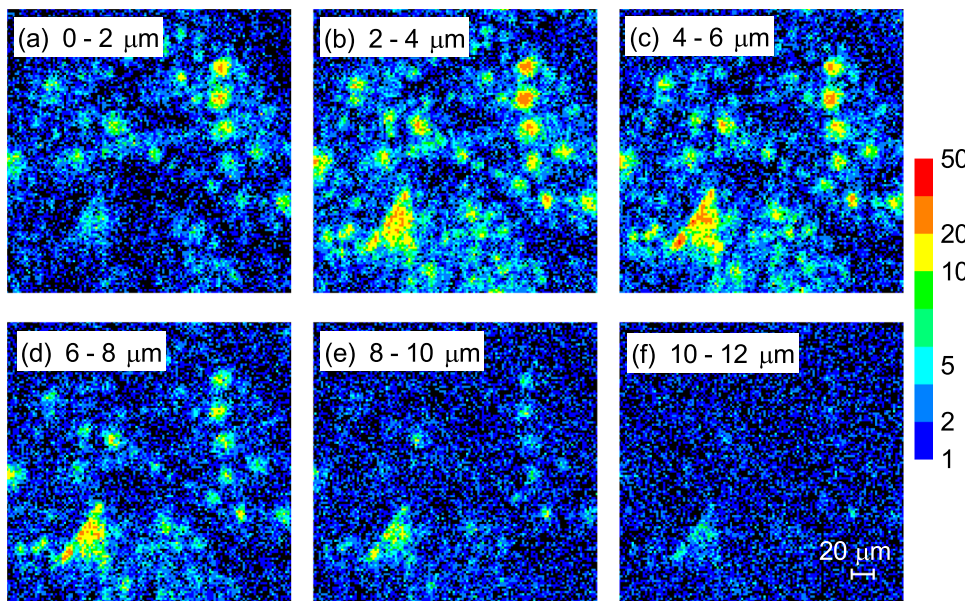


**FIG. 4.** 3-dimensional mapping of plasma-charged hydrogen in the Al sample of  $80 \mu\text{m}$  thickness, shown for the 6 slices, (a)–(f), of  $12 \mu\text{m}$  depth. The scanned area is  $250 \times 250 \mu\text{m}^2$  which is marked in yellow in Fig. 2. The lateral resolution is  $3.5 \mu\text{m}$  and the depth resolution is  $\sim 1.2 \mu\text{m}$ , see text. Note that the color scale is logarithmic and the pixels of zero count are shown in black. The average  $\text{He}^{2+}$  beam current was 80 pA and the measurement time was about 1 hour.

$\sim 1.2 \mu\text{m}$ , as already mentioned. In Fig. 4, there are bright spots of 10–20  $\mu\text{m}$  diameter which are identified to be aggregates of hydrogen, i.e., hydrogen bubbles in the present case. It is noted that hydrogen bubbles of similar size can be formed on an Al surface when it is plasma-charged with hydrogen at room temperature.<sup>16</sup> The brightness of each spot in Fig. 4 changes with increasing the depth, reflecting the shape of the bubble. These bubbles are localized in the surface layer of about 12  $\mu\text{m}$  thickness. When we observe the maps in detail, the bubbles seem to be aligned or distributed regularly. The underlying mechanism for such distribution of bubbles might be related with micro-structure, for example, grain boundaries, of the sample.

In the 6 maps in Fig. 4, there lies a uniform yield of dominantly 0 or 1 counts under the yield of hydrogen aggregates. This uniform yield originates not only from the background probably due to nuclear reactions, mentioned earlier, but also from small clusters of hydrogen. From Fig. 3, the ratio of total hydrogen yield to background yield, i.e., the signal-to-noise ratio, can be determined from the area under the spectrum for the 0–12  $\mu\text{m}$  depth. It follows from this ratio of 2.40 that 34% of the uniform yield is the hydrogen yield, while 66% is the background yield. This leads to another conclusion that 79% of the total hydrogen in the Al sample forms the bubbles of observable sizes, while 21% remains in smaller clusters that cannot be resolved in the present T-ERDA. The integrated uniform yield over each map is approximately equal to the same amount of  $(1.20 \pm 0.07) \times 10^4$  counts. Since the background yield per pixel in the 6 maps is sufficiently low, i.e., at most  $12700 \times 0.66/128^2 = 0.51$  counts, the maps in Fig. 4 suffer only negligible influence of the background.

The present experimental results allow to determine the critical hydrogen concentration  $n_c$  minimally needed for growth of the bubbles of ten- $\mu\text{m}$  size. Actually, looking at the 6 maps in Fig. 4 from (a) to (f), we notice rather abrupt disappearance of the bubble images between (d) and (f). Therefore, the hydrogen concentration for map (e) gives the critical condition for formation of the bubbles. By the same procedure as that to obtain  $n_{av}$  from Eq. (1), we have obtained  $n_c = 1.6 \times 10^{20} \text{cm}^{-3}$  ( $Y = 9746$  counts and  $t = 2 \mu\text{m}$  in this case), which corresponds to 0.27% of the atomic density of polycrystalline Al.

#### IV. CONCLUSIONS

The 3-dimensional hydrogen distribution in H-charged Al has been observed nondestructively using T-ERDA. The set of

depth-dependent distribution maps of hydrogen has visualized the hydrogen bubbles in Al. Furthermore, from the quantitative analysis of the data we have determined not only the average hydrogen concentration but also the critical hydrogen concentration for growth of the bubbles of ten- $\mu\text{m}$  size. T-ERDA combined with nuclear elastic scattering thus provides direct information about microscopic behavior of hydrogen in materials.

#### ACKNOWLEDGMENTS

The authors thank the technical staff at UTTAC for supplying the high-quality He beam of  $\mu\text{m}$  size. This work was supported in part by Cross-ministerial Strategic Innovation Promotion Program – Unit D66 – Innovative measurement and analysis for structural materials (SIP-IMASM) operated by the cabinet office.

#### REFERENCES

- <sup>1</sup>J. B. Condon and T. Schober, *J. Nucl. Mater.* **207**, 1 (1993).
- <sup>2</sup>S. K. Dwivedi and M. Vishwakarma, *Int. J. Hydrogen Energy* **43**, 21603 (2018).
- <sup>3</sup>F. A. Stevie, *Surf. Interface Anal.* **48**, 310 (2016).
- <sup>4</sup>M. Koyama, M. Rohwerder, C. C. Tasan, A. Bashir, E. Akiyama, K. Takai, D. Raabe, and K. Tsuzaki, *Materials Science and Technology* **33**, 1481 (2017).
- <sup>5</sup>A. Griesche, E. Dabah, T. Kannengiesser, N. Kardjilov, A. Hilger, and I. Manke, *Acta Mater.* **78**, 14 (2014).
- <sup>6</sup>P. Reichart, G. Datzmann, A. Hauptner, R. Hertenberger, C. Wild, and G. Dollinger, *Science* **306**, 1537 (2004).
- <sup>7</sup>K. Peeper, M. Moser, P. Reichart, E. Markina, M. Mayer, S. Lindig, M. Balden, and G. Dollinger, *J. Nucl. Mater.* **438**, S887 (2013).
- <sup>8</sup>C. E. Buckley, H. K. Birnbaum, J. S. Lin, S. Spooner, D. Bellmann, P. Staron, T. J. Udovic, and E. Hollar, *J. Applied Crystallography* **34**, 119 (2001).
- <sup>9</sup>C. E. Buckley and H. K. Birnbaum, *J. Alloys and Compounds* **330-332**, 649 (2002).
- <sup>10</sup>T. Izumi and G. Itoh, *Materials Transactions* **52**, 130 (2011).
- <sup>11</sup>M. S. Bhuiyan, H. Toda, Z. Peng, S. Hang, K. Horikawa, K. Uesugi, A. Takeuchi, N. Sakaguchi, and Y. Watanabe, *Materials Science and Engineering A* **655**, 221 (2016).
- <sup>12</sup>A. Yamazaki, H. Naramoto, K. Sasa, S. Ishii, S. Tomita, M. Sataka, H. Kudo, M. Ohkubo, and A. Uedono, *Nucl. Instrum. Meth. Phys. Res. B* **450**, 319 (2019).
- <sup>13</sup>J. F. Ziegler and J. P. Biersack, SRIM2013, The Stopping and Range of Ions in Matter, <http://www.srim.org/>.
- <sup>14</sup>IBANDL (Ion Beam Analysis Nuclear Data Library), <https://www-nds.iaea.org/exfor/iband.htm>.
- <sup>15</sup>G. Hupin, S. Quaglioni, and P. Navrtil, *Phys. Rev. C* **90**, 061601 (2014).
- <sup>16</sup>D. Milcius, L. L. Pranevicius, and C. Templier, *J. Alloys Comp* **398**, 203 (2005).